



## Article

# Numerical Analysis of Leakage and Diffusion Characteristics of In-Situ Coal Gas with Complex Components

Enbin Liu <sup>1,\*</sup> , Lianle Zhou <sup>1</sup>, Ping Tang <sup>2</sup>, Bo Kou <sup>3</sup>, Xi Li <sup>1</sup> and Xudong Lu <sup>1</sup> 

<sup>1</sup> Petroleum Engineering School, Southwest Petroleum University, Chengdu 610500, China; 202221000801@stu.swpu.edu.cn (L.Z.); 202221000780@stu.swpu.edu.cn (X.L.); 202121000947@stu.swpu.edu.cn (X.L.)

<sup>2</sup> Southwest Oil and Gas Field Company, PetroChina, Research Institute of Gathering and Transportation Engineering Technology, Chengdu 610500, China; tang1293@petrochina.com.cn

<sup>3</sup> PipeChina Yunnan Company, Kunming 650214, China; 202022000761@stu.swpu.edu.cn

\* Correspondence: enbin.liu@swpu.edu.cn

**Abstract:** To alleviate the shortage of natural gas supply, the in-situ conversion of coal to natural gas is more beneficial for advancing the clean and efficient use of energy. Since in-situ coal gas contains complex components, such as H<sub>2</sub>, CH<sub>4</sub>, and CO, their leakage poses a serious risk to human life and property. Currently, the area of consequence of the harm caused by a leak in a gathering pipeline transporting in-situ coal gas has not been clarified. Therefore, this paper adopted the method of numerical simulation to pre-study the concentration distribution of each component and determined that the main components of concern are CO and H<sub>2</sub> components. Afterward, the diffusion law of in-situ coal gas is analyzed and studied under different working conditions, such as wind speed, temperature, pipe diameter, leakage direction, and leakage aperture ratio. The results indicate that when a pipeline leak occurs, the CO component has the largest influence range. With increasing wind speed, the warning boundary of CO rapidly expands downwind, then gradually diminishes, reaching a peak value of 231.62 m at 7 m/s. The range of influence of the leaked gas is inversely proportional to temperature and directly proportional to pipe diameter and leakage aperture ratio. When the gas leaks laterally, the diffusion early warning boundary value of each component is maximal. Among them, the leakage aperture ratio has a significant impact on the concentration distribution of in-situ coal gas, whereas the effect of temperature is relatively minor. This study contributes to an understanding of the leakage and diffusion characteristics of in-situ coal gas-gathering pipelines.

**Keywords:** in-situ coal gas; diffusion pattern; numerical study; diffusion early warning boundary; pipeline leakage



**Citation:** Liu, E.; Zhou, L.; Tang, P.; Kou, B.; Li, X.; Lu, X. Numerical Analysis of Leakage and Diffusion Characteristics of In-Situ Coal Gas with Complex Components. *Energies* **2024**, *17*, 4694. <https://doi.org/10.3390/en17184694>

Academic Editor: Kalyan Annamalai

Received: 29 July 2024

Revised: 12 September 2024

Accepted: 18 September 2024

Published: 20 September 2024



**Copyright:** © 2024 by the authors. Licensee MDPI, Basel, Switzerland. This article is an open access article distributed under the terms and conditions of the Creative Commons Attribution (CC BY) license (<https://creativecommons.org/licenses/by/4.0/>).

## 1. Introduction

With the rapid growth in global demand for natural gas and hydrogen, the development of effective gas transportation technologies has become increasingly important [1]. In-situ coal gasification, as an emerging energy conversion method, can convert coal into combustible gases underground, thus addressing the environmental issues posed by traditional energy supplies [2–4]. However, the complex composition of in-situ coal gas (ISCG), which includes H<sub>2</sub>, CO, and CH<sub>4</sub>, complicates its diffusion characteristics and potential hazards during transport more than those of traditional gases [5–7].

In recent years, innovative configurations of gas pipelines have gradually become a research hotspot [8–10]. Some new pipeline designs, such as high-pressure hydrate pipelines or multiphase flow transportation systems, not only improve gas transportation efficiency but may also enhance the production efficiency of in-situ coal gas [11–13]. However, research on the leakage and diffusion characteristics of these innovative configurations remains insufficient. Li et al. [14] established a predictive model using a backward propagation neural network (BPNN) to determine the maximum horizontal dispersion distance of

mixed hydrogen and natural gas released from three pipeline leak sources. This model was used to predict the maximum horizontal hazard distance. Berstad et al. [15] considered the effect of fluid leakage through crack openings as a source term included in one-dimensional fluid equations. While this model aligned well with experiments, it remains limited to ideal gas conditions. Consequently, Morin et al. [16] proposed a numerical model based on this to assess the ductile fracture of carbon dioxide transportation pipelines under phase change and two-phase flow conditions.

When gas leaks occur due to the complexity of ISCG components, there are multiple potential hazards, such as combustibility, explosiveness, toxicity, and asphyxiation. Therefore, the complexity of ISCG leakage diffusion far exceeds that of gases like natural gas or hydrogen [17,18]. Numerous scholars have conducted extensive research on the effects of diffusion of leakage gas from pipelines on explosivity and toxicity. Oke et al. [19] established a numerical model based on the characteristic method to predict the release rate of high-pressure hydrocarbons after pipeline leaks. They considered the radial and axial fluid movement near the leak hole, as well as the transient leak rate at the leak hole. To determine leak scenarios in two and three dimensions, Moghadam et al. [20] presented formulae for the estimation of the amount of gas leakage from buried medium- and low-pressure pipelines. Mahgerefteh et al. [21] studied the diffusion of leaks in three pipeline systems: a three-branch pipeline, a bend, and a straight pipe to ascertain the impact of the pipeline structure on leaks. The results revealed that the pipeline structure has minimal impact on the leakage volume. Despite significant progress in combustible gas pipeline leakage diffusion models, numerous issues remain, particularly in the field of leakage diffusion research for ISCG gathering pipelines, necessitating more comprehensive and in-depth theoretical model research.

Many factors contribute to the diffusion of ISCG gasification leaks. Previous studies have focused on the regulatory aspects of gas leakage diffusion, primarily concerning gas properties, environmental factors, and pipeline characteristics. Terrain and atmospheric conditions affect dispersion behavior. Scargiali et al. [22] conducted simulations on heavy gas cloud dispersion over large and complex terrains, noting the substantial influence of atmospheric stability and terrain conditions on ground gas concentration distribution. Zhu et al. [23] found that all environmental dispersion factors, except humidity, affect the distance of the combustible vapor cloud, with the gas source release factor having a more significant impact. Liu et al. [24] studied the diffusion of natural gas pipeline leaks under different layouts, observing that enclosed layouts exhibit the most effective wind-blocking effects. Moreover, the diffusion patterns of different gases vary significantly. Holborn et al. [25] analyzed the large-scale leakage of liquid hydrogen, demonstrating that the leakage rate and duration are the primary determinants of the shape of the combustible mass curve. Wang et al. [26] simulated changes in natural gas concentration under various leakage conditions. The results show that key parameters such as leakage hole size, leakage hole location, and soil properties greatly influence the gas diffusion process. Building upon the understanding of natural gas pipeline leakage diffusion, Zhu et al. [27] examined the leakage diffusion behavior and concentration distribution of blended-hydrogen natural gas pipelines under different blending ratios, release pressures, and leakage directions. Although several studies have explored the diffusion characteristics of gas leaks, the existing literature primarily focuses on the behavior of single-component gases, lacking in-depth analysis of multi-component ISCG gas systems.

The existing literature predominantly focuses on the behavior of single-component gases, lacking an in-depth analysis of multi-component gas systems. This study employs numerical simulation methods to analyze the effects of various environmental conditions (such as wind speed, temperature, and pipe diameter) on leakage and diffusion behaviors. These investigations fill a gap in the current literature, especially considering the complex components of in-situ coal gas ( $H_2$ ,  $CH_4$ ,  $CO$ ), thereby providing a reference for safety monitoring.

## 2. Methods

### 2.1. Physical Model

Considering the relatively high operating pressure of an in-situ coal gas pipeline in Ordos, studying leakage diffusion requires a large fluid domain. Simultaneously, to more accurately reflect the leakage diffusion process of ISCG, this paper utilized SpaceClaim (2021 R2) software to establish a three-dimensional geometric model of the fluid domain, as shown in Figure 1. To ensure that the gas can fully develop within the pipeline and the surrounding air, the dimensions of the computational domain are set to a length of 1000 m, a width of 40 m, and a height of 40 m [28,29]. The leak hole is located at the center of the pipeline and is oriented vertically to the ground, with the left side wall serving as the boundary condition for wind speed. The leaking gas interacts with the wind speed as it flows through the computational domain. The diameters of the pipeline and the leak hole depend on the operating conditions.

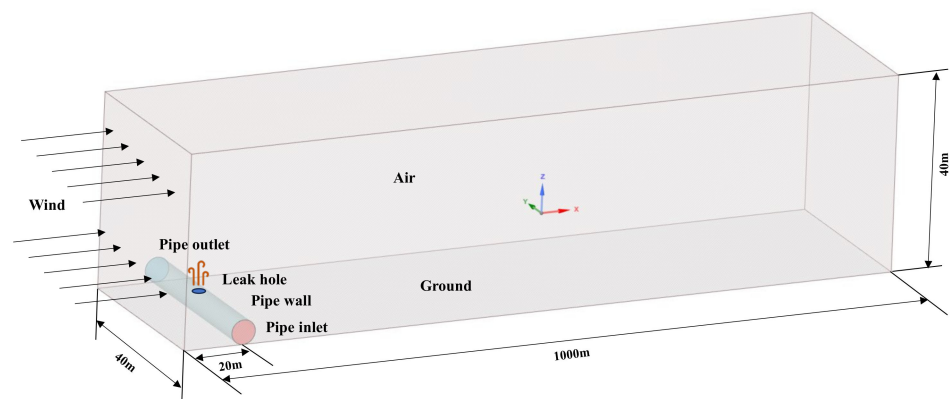


Figure 1. Geometrical modeling of leakage diffusion in ISCG gathering pipelines.

### 2.2. Mathematical Model

To clarify the CFD method, this study presents the numerical model and its solution process in Figure 2. The figure outlines the complete workflow from the model establishment to final data processing, aiding readers in quickly understanding our methodology. The numerical simulation in this article was conducted in a Linux CentOS 7 environment (CentOS Project, Raleigh, NC, USA). The CPU used is the AMD EPYC 7763 processor (AMD, Santa Clara, CA, USA), which has 128 cores. The memory consists of Samsung DDR4 16 GB ECC Registered 3200 MHz server memory modules (Samsung Electronics, Suwon, Republic of Korea), totaling 256 GB.

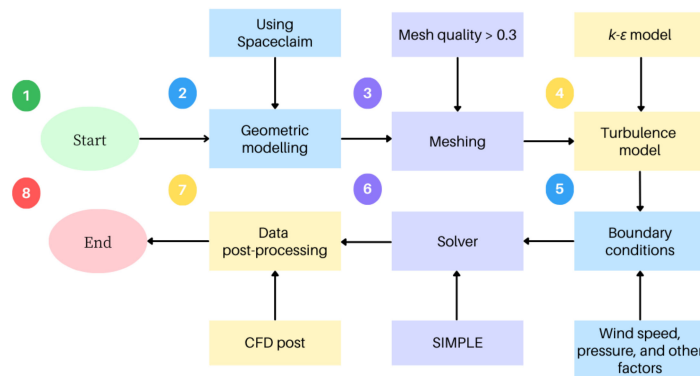


Figure 2. Flowchart of CFD method.

#### 2.2.1. Control Equation

The leakage of an ISCG pipeline is an exceedingly complex process. Assuming no change in the cross-section of the ISCG gathering pipeline during the leakage process, there

is no chemical reaction between the leaking ISCG and the air. Also, the pressure inside the pipeline and the shape and area of the rupture remain unchanged. Based on the above, the following equations are established [30,31].

### (1) Continuity Equation

Assuming that the cross-section of the in-situ coal gasification transportation pipeline does not change during a leak, the continuity equation for ISCG leakage can be derived based on mass conservation as follows:

$$\frac{\partial \rho}{\partial t} + \frac{\partial(\rho u_i)}{\partial x_i} = 0 \quad (1)$$

### (2) Energy Equation

Based on the law of conservation of energy, the energy equation established by fluid dynamics is

$$\frac{\partial}{\partial t}(\rho E) + \nabla[\vec{u}(\rho E + p)] = \nabla \left( k_{eff} \nabla \cdot T - \sum_f h_f J_f + (\tau_{eff} \cdot \vec{u})_{eff} \right) + S_k \quad (2)$$

### (3) Momentum Equation

The equation of motion of the ISCG is based on Newton's second law, and its expression is shown in Equation (3):

$$\frac{\partial(\rho u_i)}{\partial t} + \frac{\partial}{\partial x_j}(\rho u_i u_j) = -\frac{\partial p}{\partial x_i} + \frac{\partial}{\partial x_j} \left( \mu \frac{\partial u_i}{\partial x_j} \right) + \rho g + F_i \quad (3)$$

where  $\rho$  is the density of ISCG,  $\text{kg}/\text{m}^3$ ;  $t$  is the time,  $s$ ;  $u_i$  is the velocity in the three directions of  $x$ ,  $y$ , and  $z$ ;  $E$  is the total energy of the microcluster;  $h$  is the enthalpy of the ISCG;  $k_{eff}$  is the effective thermal conductivity of the ISCG;  $J_f$  is the diffusive flux of the components;  $S_k$  is the contribution from external heat sources;  $P$  is the operating pressure;  $g$  is the gravitational acceleration of the ISCG;  $\mu$  is the viscosity of the ISCG;  $F_i$  is the body force.

## 2.2.2. Component Transport Model

The leakage diffusion process of the ISCG gathering pipeline needs to satisfy the laws of mass conservation, energy conservation, and momentum conservation. In addition, to investigate the leakage diffusion issue of ISCG from the gathering pipeline into the atmospheric space, this paper utilizes component transport equations to calculate and analyze its leakage diffusion and transport behavior. The expression for this equation is as follows [32,33]:

$$\frac{\partial}{\partial t}(\rho Y_i) + \nabla \cdot (\rho \bar{v} Y_i) = -\nabla \bar{J}_i + R_i + S_i \quad (4)$$

$$\bar{J}_i = -\left( \rho D_{i,m} + \frac{\mu_t}{Sc_i} \right) \nabla Y_i \quad (5)$$

$$Sc_i = \frac{\mu_t}{\rho D_t} \quad (6)$$

where  $Y_i$  is the mass fraction of each component of the ISCG;  $R_i$  is the generation rate of each component of the ISCG;  $S_i$  is the additional generation rate due to each component of the ISCG;  $\bar{J}_i$  is the diffusive flux of each component of the ISCG;  $D_{i,m}$  is the diffusivity of each component of the ISCG;  $Sc_i$  is the Schmitt number of each component of the ISCG;  $\mu_t$  is the kinetic viscosity of the turbulence;  $D_t$  is the turbulent diffusivity.

## 2.2.3. Turbulence Model

This study employs the Realizable  $k-\varepsilon$  turbulence model, which is widely used in numerical simulations of gas leakage and diffusion due to its excellent performance in handling complex flow and high curvature problems. Compared to the standard  $k-\varepsilon$

model, the Realizable  $k-\varepsilon$  model is more effective at capturing turbulent characteristics, particularly in regions with high gradients. This makes it suitable for analyzing the airflow distribution and diffusion characteristics of in-situ coal gas leakage in our research. According to [34–36],

$$\frac{\partial(\rho k)}{\partial t} + \frac{\partial(\rho k u_i)}{\partial x_i} = \frac{\partial}{\partial x_j} \left[ \left( \mu + \frac{\mu_t}{\sigma_k} \right) \frac{\partial k}{\partial x_j} \right] + G_k + G_b - \rho \varepsilon - Y_M + S_k \quad (7)$$

$$\frac{\partial(\rho \varepsilon)}{\partial t} + \frac{\partial(\rho \varepsilon u_i)}{\partial x_i} = \frac{\partial}{\partial x_j} \left[ \left( \mu + \frac{\mu_t}{\sigma_\varepsilon} \right) \frac{\partial \varepsilon}{\partial x_j} \right] + \rho C_1 S \varepsilon - \rho C_2 \frac{\varepsilon^2}{k + \sqrt{\nu \varepsilon}} + C_{1\varepsilon} \frac{\varepsilon}{k} C_{3\varepsilon} G_b + S_\varepsilon \quad (8)$$

where  $C_1 = \max\left[0.43, \frac{\eta}{\eta+5}\right]$ ,  $\eta = S \frac{k}{\varepsilon}$ ,  $S = \sqrt{2S_{ij}S_{ij}} \cdot u_i$  is the velocity in the direction of grid;  $i$  in the discrete computation;  $x_i$  and  $x_j$  are the directions of grids  $i$  and  $j$  in the discrete computation;  $G_k$  is the turbulent kinetic energy induced by the mean velocity gradient;  $G_b$  the turbulent kinetic energy induced by the buoyancy force;  $Y_M$  is the effect of the pulsating expansion of compressible turbulence on the total dissipation rate;  $\sigma_k$  and  $\sigma_\varepsilon$  are the Prandtl numbers corresponding to  $k$  and  $\varepsilon$ ;  $C_2$ ,  $C_{1\varepsilon}$ , and  $C_{3\varepsilon}$  are the default empirical constants.

#### 2.2.4. Pipe Leakage Model

For the small orifice leak model ( $d/D \leq 0.2$ ) and the large orifice leak model ( $0.2 < d/D \leq 0.8$ ), the leakage velocity is calculated according to Equation (9):

$$u = \frac{C_0 P_i}{\rho_i} \sqrt{\frac{M}{ZRT_i} \cdot k \cdot \left( \frac{2}{k+1} \right)^{\frac{k+1}{k-1}}} \quad (9)$$

For the full-scale leakage model, the leakage velocity of the gathering pipeline is calculated according to Equation (10):

$$u_3 = u_2 = \frac{\rho_1 u_1}{\rho_2} \quad (10)$$

where  $d$  is the diameter of the leakage hole;  $D$  is the inner diameter of the pipe;  $k$  is the adiabatic index of the ISCG;  $P_i$  is the pressure at position  $i$ ;  $T_i$  is the temperature at position  $i$ ;  $\rho_i$  is the density at position  $i$ ;  $M$  is the molar mass;  $C_0$  is the leakage coefficient;  $u_i$  is the velocity at position  $i$ .

### 2.3. Boundary Conditions and Meshing

#### 2.3.1. Boundary Conditions

The ISCG gathering pipeline transports an average of 200,000 cubic meters of gas per day, with a pipe diameter of 114.3 mm, a pipeline operating pressure of 5.7 MPa, a temperature inside the pipe of 300 K, and an average temperature of the outside environment of 290 K. Wherein the components of the ISCG are shown in Table 1.

**Table 1.** Component of the ISCG.

Component	CH <sub>4</sub>	CO <sub>2</sub>	CO	H <sub>2</sub>	C <sub>2</sub> H <sub>6</sub>
Mole fraction	0.370	0.410	0.050	0.150	0.020
Mass fraction	0.226	0.686	0.530	0.012	0.023

Five factors, namely wind speed, temperature, leakage direction, pipe diameter, and leak aperture ratio, were selected to investigate the leakage diffusion law of ISCG gathering pipelines. The temperature values at each outlet surface are uniformly set to 290 K, and the outlets are defined using turbulence intensity and hydraulic diameter. The specific boundary condition settings are shown in Table 2.

**Table 2.** Boundary condition.

Location	Boundary Type
Hole	Velocity-Inlet
Pipeline	Wall
Left wall	Velocity-Inlet/Pressure-Outlet
Top wall	Pressure-Outlet
Right wall	Pressure-Outlet
Ground	Wall

### 2.3.2. Grid Independent Verification

In the simulation of leakage diffusion in the gathering pipeline, three working conditions of small hole leakage, large hole leakage, and full-size leakage are studied. The hole sizes are 11.43 mm, 57.15 mm, and 114.3 mm, respectively. In the meshing process, overall meshing and local encryption of the leakage holes are used to complete the meshing, in which the mesh model of the large hole leakage is shown in Figure 3. The minimum mesh quality is 0.3, the maximum mesh aspect ratio is 9.50, and the maximum mesh skewness is 0.69. Therefore, the mesh quality of the model in this study meets the simulation requirements for numerical research.

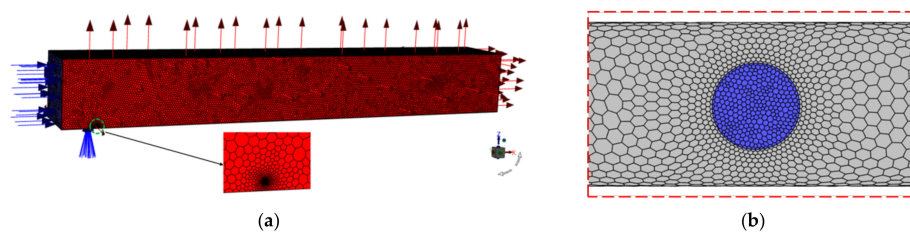


**Figure 3.** Fluid domain meshing and local encryption. (a) Fluid domain model mesh. (b) Localized encryption of mesh at leakage holes.

To balance computational accuracy and load, this paper extracted CO<sub>2</sub> concentration data from the monitoring point located downwind of the leakage orifice at (50, 0, 2) for grid independence verification and time step independence verification. The computational results are illustrated in Figure 4.

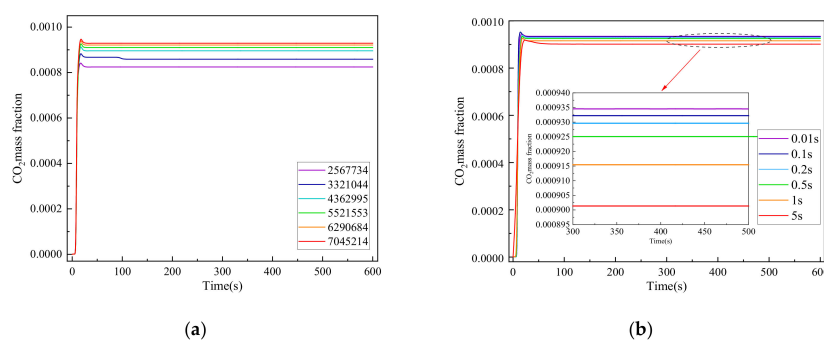


**Figure 4.** Model independence verification. (a) Grid independence verification. (b) Time step independence verification.

From Figure 4, it is evident that when the number of grids is less than 5,521,553, changes in the grid count significantly impact the distribution of CO<sub>2</sub> concentration and a minor increase in concentration as the grid count rises. However, when the grid count exceeds 5,521,553, the difference in CO<sub>2</sub> concentration becomes minimal, with a similar trend in variation. For time steps not exceeding 0.5 s, the change in CO<sub>2</sub> concentration is minimal, but when surpassing 0.5 s, there is a significant variation in CO<sub>2</sub> concentration. Therefore, the final simulation calculation will employ 5,521,553 grids and a time step of 0.5 s.

### 3. Results and Discussion

#### 3.1. Investigation of the Diffusion Patterns in Standard Leakage Conditions

To more intuitively study the diffusion patterns of leaks, a combined consideration of 20% of the lower explosive limit (LEL) and the occupational exposure limit (OEL) for hazardous gases was adopted. The smaller value between these two limits was taken as the threshold for the diffusion early warning boundary (DEWB) of each component, as shown in Table 3.

**Table 3.** Threshold values for diffusion early warning boundary (DEWB) of each component.

Component	CH <sub>4</sub>	C <sub>2</sub> H <sub>6</sub>	H <sub>2</sub>	CO	CO <sub>2</sub>
LEL	5%	3%	4%	12.5%	-
OEL	-	-	-	0.0024%	0.05%
Threshold values for DEWB	1%	0.6%	0.8%	0.0024%	0.05%

Considering the complex composition of the ISCG, for ease of analysis, this paper conducted a preliminary study on the concentration distribution of each component to determine the main focus components for subsequent study. The wind speed of 7 m/s and large hole leakage were used as the standard working conditions for the study. Among the simulation results, the process of the 600 s leakage was taken for analysis. The specific concentration distribution is shown in Figure 5.

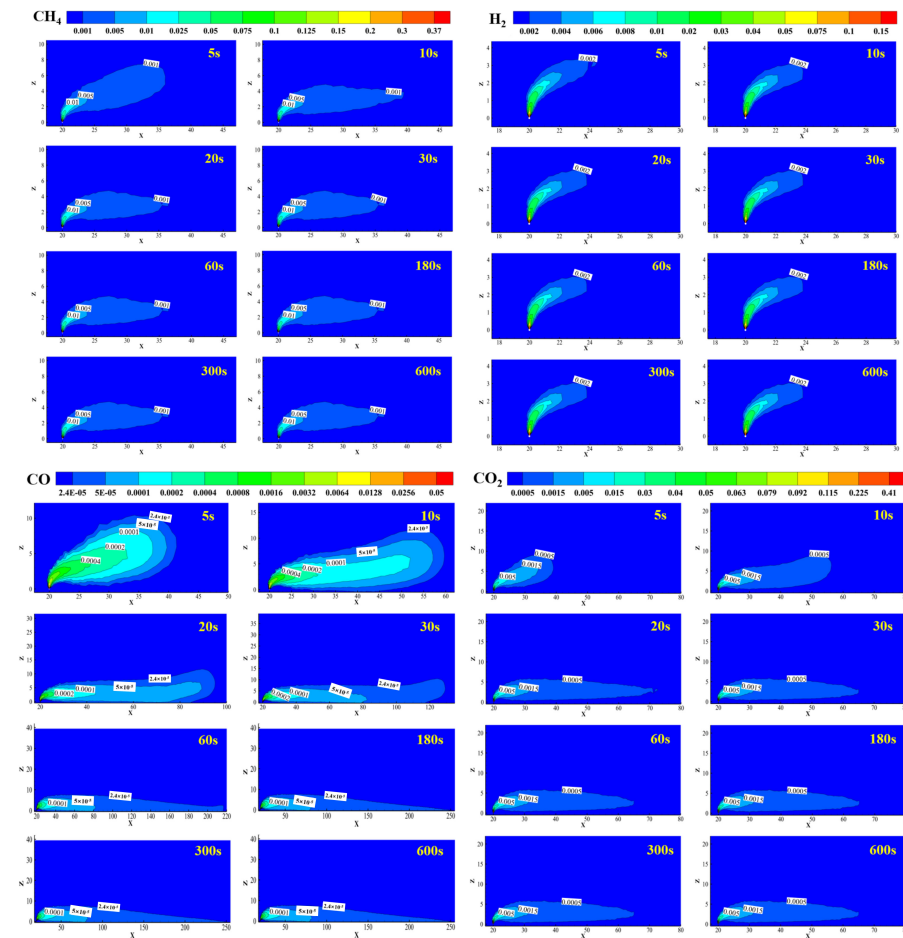


**Figure 5.** Concentration distribution of various components in the ISCG (Y = 0 m section).

As shown in Figure 5, when leakage occurs in the pipeline, the DEWB of each component is not identical, as well as the time for the different warning boundaries of the

components to stabilize changes. Due to the low thresholds for CO, the range of influence of CO is the largest. Therefore, subsequent study of the leakage diffusion law mainly focuses on this component. Considering the significant differences in properties such as density, explosive limits, and diffusion rates between H<sub>2</sub> and other components, it is necessary to analyze and evaluate the concentration distribution of this component.

### 3.2. Influence of Wind Speed

The diffusion of a gas leak is affected by many factors, with wind speed being a significant one.

Figure 6 shows the non-stationary variation of ISCG concentration at different wind speeds. From the graph, it can be seen that with increasing wind speed, the DEWB for CO initially increases and then decreases, while the DEWB for H<sub>2</sub> exhibits a slow upward trend. During the initial stage of leakage, the ISCG experiences high jet velocity and jet pressure; thus, the impact of wind speed on gas distribution is not particularly pronounced. Nonetheless, after a period of time, the direction of jet gas movement undergoes significant deflection. This phenomenon occurs because the initial kinetic energy of the ISCG progressively diminishes during thorough mixing with air, leading to wind gradually becoming the dominant factor influencing gas diffusion. As a result, under the influence of wind, the leaked gas continuously tilts downwind, and with increasing radial distance, this tilting tendency gradually intensifies. Once the wind speed reaches a certain level, the ISCG accelerates its downwind diffusion, causing CO concentration to dilute below the DEWB threshold. Thus, with a further increase in wind speed, the impact range of the CO gas cloud continually diminishes.

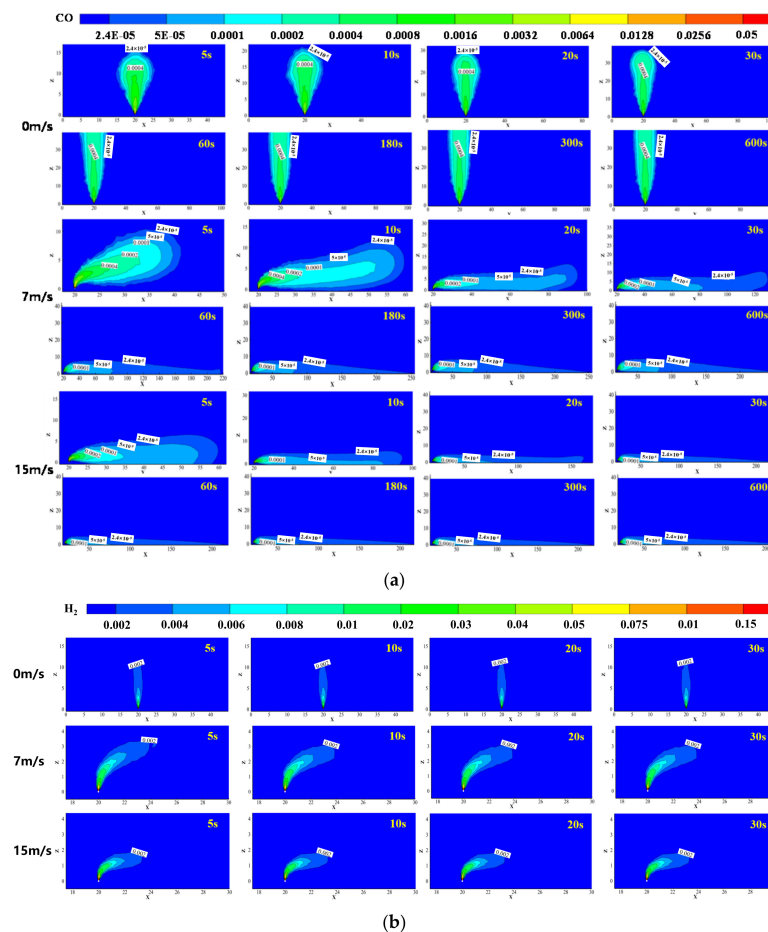


**Figure 6.** Planar concentration distribution of ISCG at different wind speeds. (a) Planar distribution of CO mole fraction at different wind speeds ( $Y = 0$  m section). (b) Planar distribution of H<sub>2</sub> mole fraction at different wind speeds ( $Y = 0$  m section).



As shown in Figure 7a, when the wind speed is 7 m/s, its boundary peaks at 231.62 m. From Figure 7b, it is apparent that the DEWB of CO<sub>2</sub> is inversely correlated with wind speed. The impact ranges of the other components exhibit slow growth with increasing wind speed but are significantly smaller than that of CO. Notably, the maximum impact area boundaries for CH<sub>4</sub> and H<sub>2</sub> are a mere 2.26 m and 1.18 m, respectively, much smaller compared to CO. This is due to the lower threshold and density of CH<sub>4</sub> and H<sub>2</sub>.

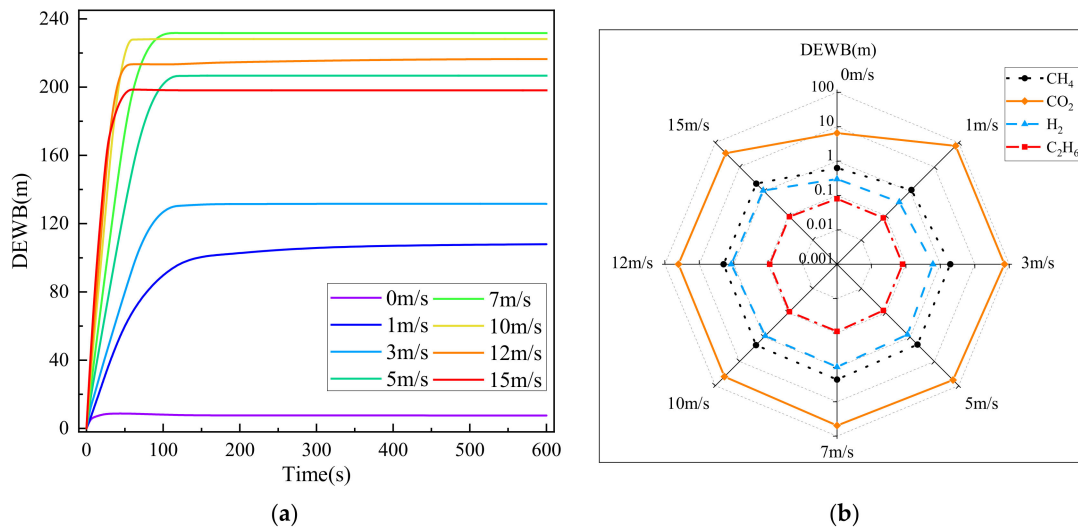


**Figure 7.** DEWB of each component at different wind speeds. (a) DEWB of the CO. (b) DEWB of the remaining components.

### 3.3. Influence of Leakage Direction

As the leakage direction is random, simulations were conducted for three different angles: 90° (lateral leakage), 45°, and 0° (longitudinal leakage). From Figure 8, when the leakage direction shifts from lateral leakage to longitudinal leakage, the CO gas cloud adopts a narrow and elongated shape, with its height increasing while the downwind impact distance decreases. For the H<sub>2</sub> component, due to the influence of density differences, the gas tends to escape upward, making it difficult to form high-concentration areas. Accordingly, during lateral leakage, the concentration peak is much lower than that of longitudinal leakage, whereas, at 45° angle leakage, the high-concentration area range falls between the two.

As shown in Figure 9, when a pipeline experiences lateral leakage, the resulting hazardous area is significantly larger than in other leakage directions because the lateral leak direction is consistent with the wind speed. Transitioning from longitudinal leakage to 45° leakage and then to lateral leakage results in a growth rate of approximately 16% in the CO impact area, with respective DEWB values of 231.62 m, 269.77 m, and 313.07 m.

### 3.4. Influence of Temperature

Temperature affects the gas properties and, hence, the diffusion pattern. Therefore, it is necessary to study the leakage diffusion pattern at different temperatures.

From Figure 10, it can be seen that when a pipeline experiences leakage, the concentration distribution of ISCG under three different temperature conditions is quite similar. This indicates that the operating temperature has an extremely limited effect on the spread distance of the leaked gas cloud. When the temperature increases from 290 K to 300 K, the DEWB for the CO gas cloud shrinks from 243.63 m to 231.62 m. With further temperature increase, this value decreases to 220.95 m again. Additionally, the two temperature increases also cause the DEWB for H<sub>2</sub> to decrease from 0.99 m to 0.94 m. This can be attributed to the fact that elevated temperatures promote turbulence in the mixed gas, resulting in enhanced diffusion and dilution effects, thereby causing a contraction of the DEWB.

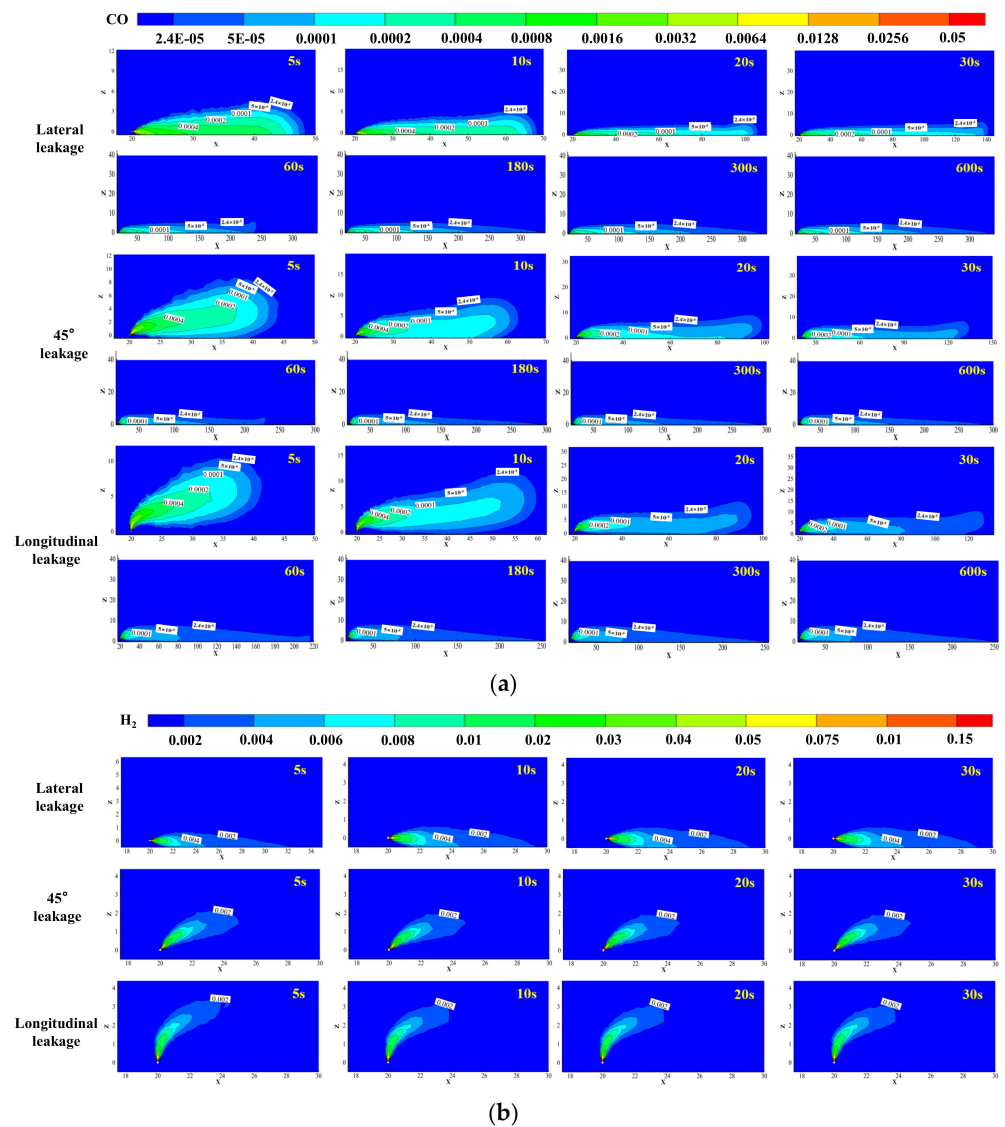


**Figure 8.** Planar concentration distribution of ISCG at different leakage directions. (a) Planar distribution of CO mole fraction at different leakage directions (Y = 0 m section). (b) Planar distribution of H<sub>2</sub> mole fraction at different leakage directions (Y = 0 m section).

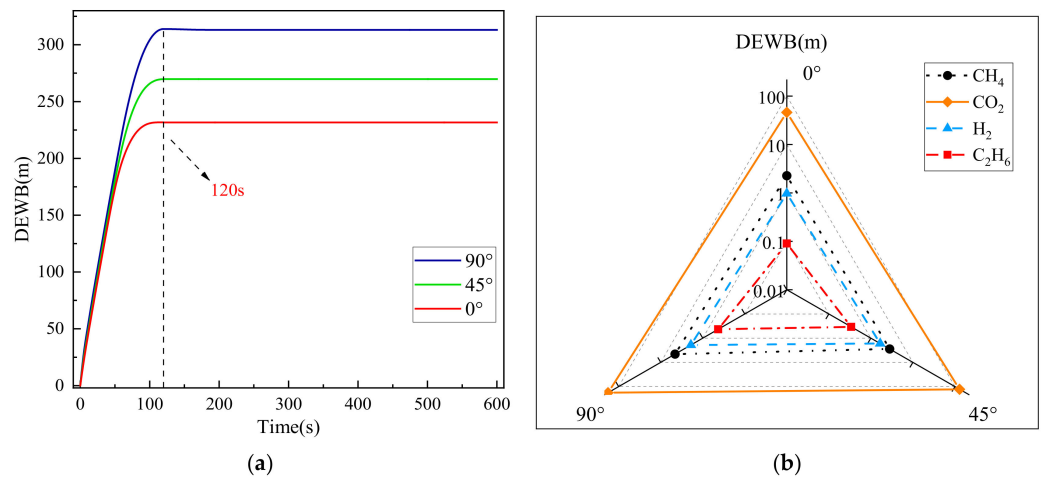
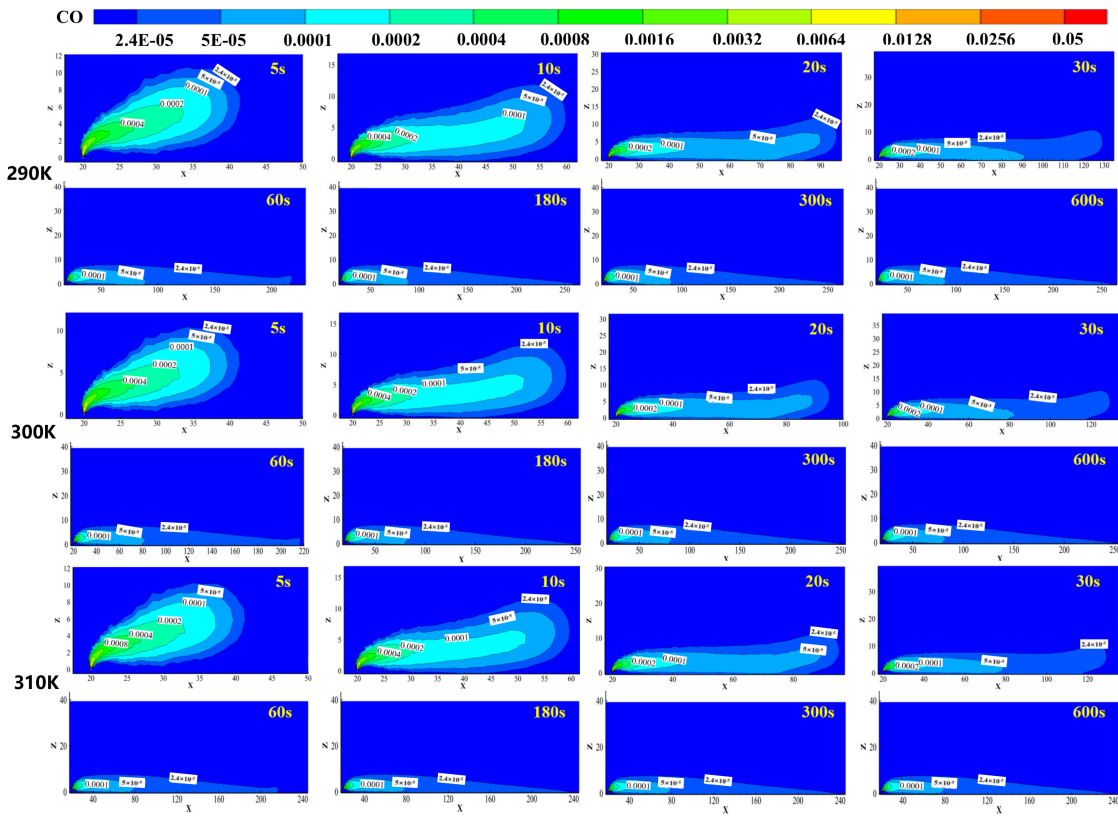
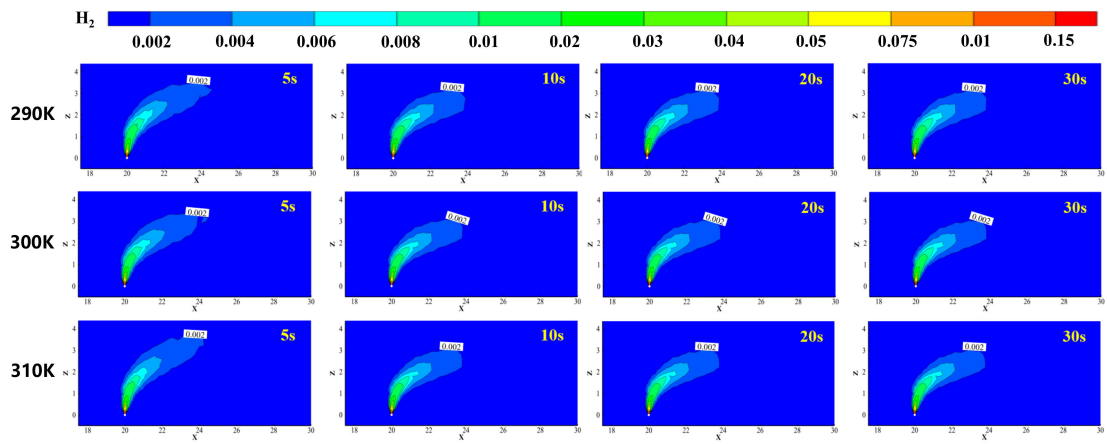


**Figure 9.** DEWB of each component at different leakage directions. (a) DEWB of the CO. (b) DEWB of the remaining components.



(a)



(b)

**Figure 10.** Planar concentration distribution of ISCG at different temperatures. (a) Planar distribution of CO mole fraction at different temperatures ( $Y = 0$  m section). (b) Planar distribution of  $H_2$  mole fraction at different temperatures ( $Y = 0$  m section).

As shown in Figure 11, analyzing the impact area boundaries of each component at different temperatures reveals that the changes in the impact range are similar across the three temperature conditions. Moreover, during the process of increasing the temperature from 290 K to 310 K, the DEWB for the CO gas cloud contracts by approximately 5% across all temperature conditions. In general, the variation in the operating temperature within the pipeline has a minimal impact on the concentration distribution range of ISCG, and temperature changes do not affect the time it takes for the leaked gas cloud to reach dynamic stability.

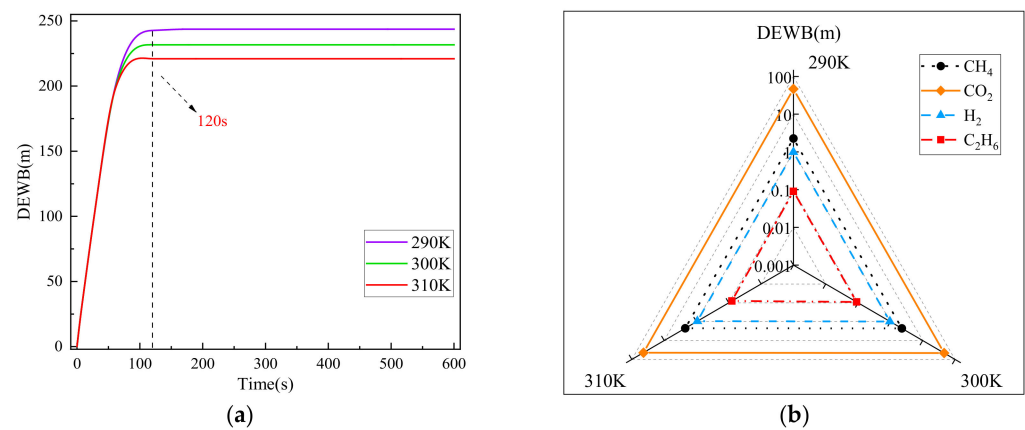


**Figure 11.** DEWB of each component at different temperatures. (a) DEWB of the CO. (b) DEWB of the remaining components.

### 3.5. Influence of Pipe Diameter

Changes in pipe diameter also affect how far the individual components of the ISCG can spread. Therefore, it is necessary to study the leakage diffusion law under different pipe diameters. Figure 12 presents the planar concentration distribution under three different leakage pipe diameters. Due to the impact of pipe diameter variation on the flow rate of the ISCG at the leakage hole, the high-concentration area of CO expands with increasing leakage pipe diameter. As the leakage continues, there is no remarkable difference in the size and shape of the CO gas cloud among the three leakage scenarios, a phenomenon that persists until around 60 s, before any noticeable changes occur. The impact range for H<sub>2</sub> slightly expands and reaches dynamic stability at 20 s, with no change in its stability time when the pipe diameter varies.

As shown in Figure 13, it is found that as the pipe diameter gradually increases, the DEWB for each component of the ISCG shows a growing trend. When the pipe diameter increases from 88.9 mm to 168.3 mm, the gas cloud radius of CO doubles. The DEWB for CO are 160.61 m, 231.62 m, and 322.00 m, while for H<sub>2</sub>, they are 0.82 m, 0.97 m, and 1.52 m, showing a significant difference compared to CO. This is due to the fact that H<sub>2</sub> accounts for only 15% of the ISCG and has a higher diffusion coefficient. In addition, the DEWB for CO<sub>2</sub> grows by 2.64 times.

### 3.6. Influence of Leakage Aperture Ratio

When leakage occurs in an ISCG pipeline, the leakage aperture ratio has a non-negligible effect on the leakage spread of the gas cloud. As shown in Figure 14, under conditions with a leakage aperture ratio of 0.1, the DEWB of the CO component experiences an abrupt increase initially, followed by a slight decrease, reaching stability at 30 s. Conversely, for leakage aperture ratios of 0.5 and 1, the leakage scenario is entirely different. With the continuation of the leakage process, the size of the CO gas cloud continuously increases, and its DEWB growth rate also continues to rise. Since H<sub>2</sub> accounts for a relatively small percentage, its DEWB is always kept within 0.2 m. Although the size of the H<sub>2</sub> gas cloud diminishes as the leakage progresses, there is a slight expansion in its DEWB.

From Figure 15, it is evident that the temporal influence range of CO exhibits a logarithmic growth trend overall, and the larger the leak hole diameter ratio, the more challenging it is for its DEWB to reach dynamic stability. For a full-scale leakage, CO requires continuous leakage for 300 s to achieve dynamic stability. Moreover, with the increase in leakage aperture ratio, the DEWB of each component increases accordingly. The DEWB of the CO component reaches a maximum of 817.99 m. In the case of the H<sub>2</sub> component, the DEWB during small hole leakage is only 0.19 m, whereas, under full-scale leakage conditions, it reaches 4.96 m, expanding by a factor of 25.11. This demonstrates

that the leakage aperture ratio has a considerable impact on the concentration distribution of gas diffusion in pipeline leakage diffusion.

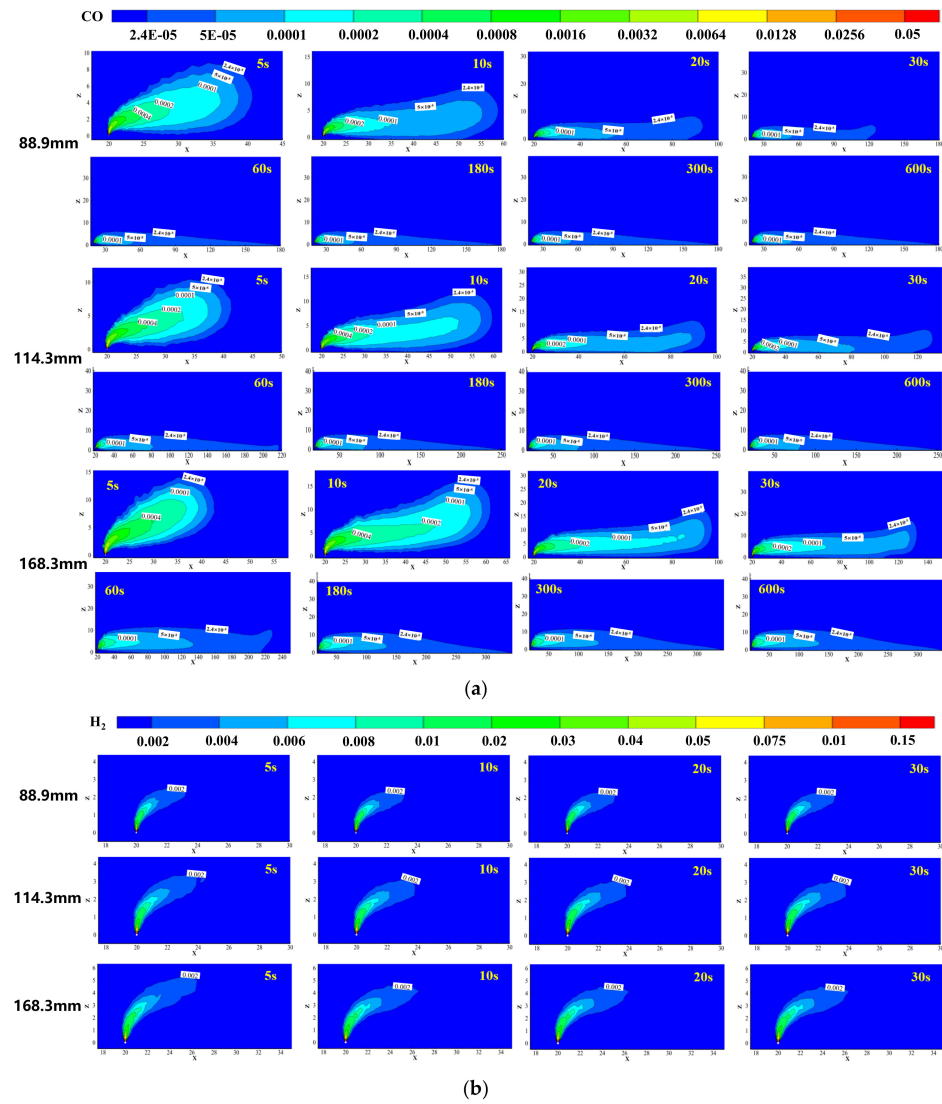


**Figure 12.** Planar concentration distribution of ISCG at different pipe diameters. (a) Planar distribution of CO mole fraction at different pipe diameters ( $Y = 0$  m section). (b) Planar distribution of H<sub>2</sub> mole fraction at different pipe diameters ( $Y = 0$  m section).

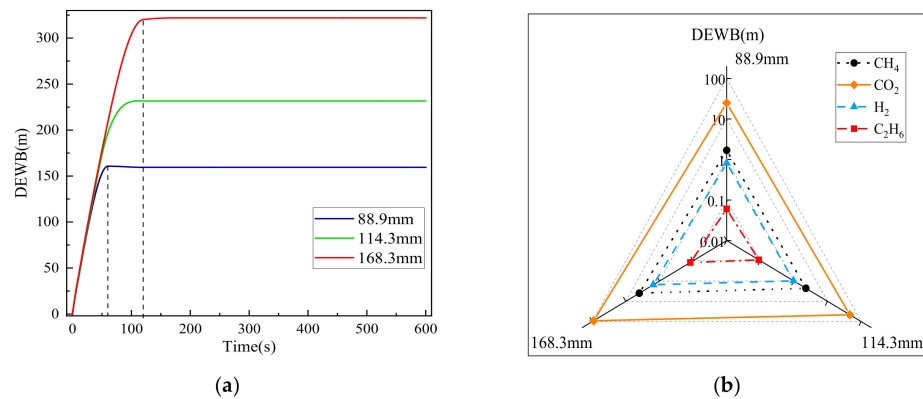


**Figure 13.** DEWB of each component for different pipe diameters. (a) DEWB of the CO. (b) DEWB of the remaining components.

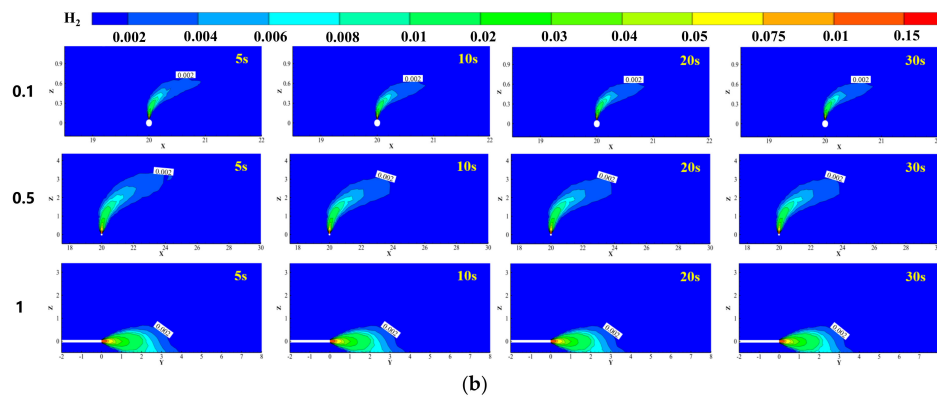
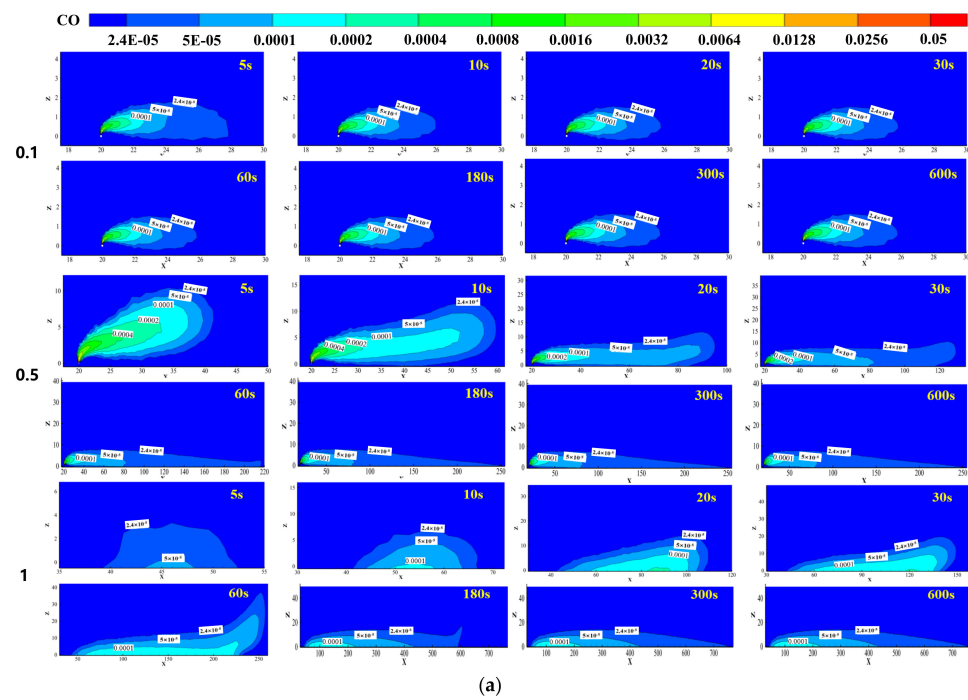


**Figure 14.** Planar concentration distribution of ISCG at different leakage aperture ratios. (a) Planar distribution of CO mole fraction at different leakage aperture ratios. (b) Planar distribution of H<sub>2</sub> mole fraction at different leakage aperture ratios.

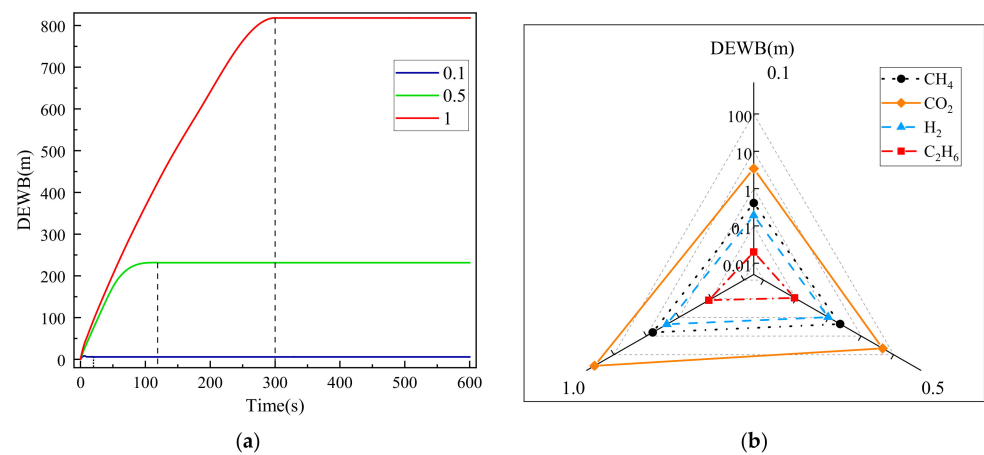


**Figure 15.** DEWB of each component at different leakage aperture ratios. (a) DEWB of the CO. (b) DEWB of the remaining components.

#### 4. Conclusions

This study investigated the influence of various factors on the diffusion behavior of the ISCG pipeline leaks. Utilizing CFD simulations, the study analyzed the impact of wind speed, leakage direction, temperature, pipe diameter, and leakage aperture ratio on the DEWB. The specific conclusions are as follows:

(1) When leakage occurs in the ISCG pipeline, the influence range of each component varies, among which the influence range of CO is the largest, far exceeding that of CH<sub>4</sub> and H<sub>2</sub>. This discovery highlights the importance of prioritizing the monitoring of CO concentration during leakage detection processes in order to take timely measures and reduce potential hazards.

(2) The results indicate that wind speed significantly affects the DEWB of CO. Higher wind speeds initially expand the DEWB due to faster gas transportation but eventually lead to a contraction due to enhanced dilution. Leakage direction also plays a crucial role, with lateral leaks resulting in larger hazardous areas compared to longitudinal leaks. Temperature's influence on DEWB is relatively minimal within the simulation range. These results underscore the necessity of considering environmental conditions and leakage direction in practical applications.

(3) Furthermore, pipe diameter and leakage aperture ratio directly correlate with the DEWB of all components. Larger diameters and leakage aperture ratios lead to larger DEWBs, particularly for CO and H<sub>2</sub>. Notably, the DEWB of H<sub>2</sub> is maximally enlarged by a factor of 25.11, and the DEWB of the CO component is even oversized by a factor of 140.52. These quantitative results emphasize the importance of paying attention to these key parameters in the design and maintenance of pipelines.

(4) This study focused on ISCG pipeline leaks under flat terrain conditions. However, there are certain limitations in this research, as it did not consider the impact of complex terrains on leakage and diffusion patterns. Future research should conduct in-depth investigations into the leakage diffusion behavior under various terrain conditions to achieve a more comprehensive understanding of how environmental factors influence the diffusion process. Additionally, empirical studies on leak detection technologies and their applicability in different environmental conditions are recommended to enhance the effectiveness of leak response.

**Author Contributions:** Conceptualization, E.L.; Methodology, B.K.; Software, E.L., L.Z. and B.K.; Formal analysis, L.Z.; Investigation, P.T. and X.L. (Xudong Lu); Resources, E.L.; Writing—original draft, L.Z.; Writing—review & editing, E.L.; Visualization, L.Z. and X.L. (Xi Li); Project administration, P.T.; Funding acquisition, E.L. All authors have read and agreed to the published version of the manuscript.

**Funding:** This work was supported by the Natural Science Foundation of Sichuan Province (2023NS-FSC0422).

**Data Availability Statement:** The original contributions presented in the study are included in the article, further inquiries can be directed to the corresponding author.

**Conflicts of Interest:** Author Ping Tang was employed by the Southwest Oil and Gas Field Company. Author Bo Kou was employed by the PipeChina Yunnan Company. The remaining authors declare that the research was conducted in the absence of any commercial or financial relationships that could be construed as a potential conflict of interest.

## Nomenclature

Symbol	Meaning
$\rho$	Density
$t$	Time
$u_i$	Velocity in the three directions of x, y, and z
$E$	Total energy of the microcluster
$k_{eff}$	Effective thermal conductivity
$J_f$	Diffusive flux of the components
$S_k$	Contribution from external heat sources
$P$	Operating pressure
$g$	Gravitational acceleration
$F_i$	Body force
$Y_i$	Mass fraction of each component
$R_i$	Generation rate of each component
$\bar{J}_i$	Diffusive flux of each component
$G_k$	Turbulent kinetic energy induced by the mean velocity gradient
$Y_M$	Effect of the pulsating expansion of compressible turbulence on the total dissipation rate
$T_i$	Temperature at position $i$

## References

- Lau, H.C.; Wang, J.; Zhang, M. A few Classification of Gas-Hydrate Deposits and Its Implications for Field-Development Potential. *SPE J.* **2021**, *26*, 3643–3667. [\[CrossRef\]](#)
- You, J.; Lee, K.J. The experimental investigation and data-driven modeling for thermal decomposition kinetics of Green River Shale. *Fuel* **2022**, *320*, 123899. [\[CrossRef\]](#)
- Ratnakar, R.R.; Gupta, N.; Zhang, K.; van Doorne, C.; Fesmire, J.; Dindoruk, B.; Balakotaiah, V. Hydrogen supply chain and challenges in large-scale LH2 storage and transportation. *Int. J. Hydrogen Energy* **2021**, *46*, 24149–24168. [\[CrossRef\]](#)
- Ren, X.; Dong, L.; Xu, D.; Hu, B. Challenges towards hydrogen economy in China. *Int. J. Hydrogen Energy* **2020**, *45*, 34326–34345. [\[CrossRef\]](#)
- Sun, Q.; Zhang, M.; Ertekin, T. The Design of Hydrogen Saline Aquifer Storage Processes Using a Machine-Learning Assisted Multiobjective Optimization Protocol. *SPE J.* **2024**, *29*, 2086–2105. [\[CrossRef\]](#)
- Delshad, M.; Alhotan, M.M.; Fernandes, B.R.B.; Umurzakov, Y.; Sepehrnoori, K. Modeling Flow and Transport in Saline Aquifers and Depleted Hydrocarbon Reservoirs for Hydrogen Energy Storage. *SPE J.* **2023**, *28*, 2547–2565. [\[CrossRef\]](#)
- Gillick, S.R.; Babaei, M. In-Situ Hydrogen Production from Natural Gas Wells with Subsurface Carbon Retention. *SPE J.* **2024**, *29*, 2119–2129. [\[CrossRef\]](#)
- You, J.; Lee, K.J. Pore-Scale Numerical Investigations of the Impact of Mineral Dissolution and Transport on the Heterogeneity of Fracture Systems during CO<sub>2</sub>-Enriched Brine Injection. *SPE J.* **2022**, *27*, 1379–1395. [\[CrossRef\]](#)
- Liu, Z.; Lin, X.; Wang, Z.; Zhang, Z.; Chen, R.; Wang, L.; Li, W. Modeling and experimental study on methane diffusivity in coal mass under in-situ high stress conditions: A better understanding of gas extraction. *Fuel* **2022**, *321*, 124078. [\[CrossRef\]](#)
- Baatar, L.; Mostaghimi, P.; Yuan, M.; Armstrong, R.T.; Adler, L.; Canbulat, I.; Si, G.; Gaidarov, B.; Jing, Y. Multiscale measurements of gas diffusion coefficient of coal using counter-diffusion and image-based methods. *Int. J. Coal Geol.* **2023**, *265*, 104155. [\[CrossRef\]](#)
- Wang, L.; Chen, J.; Ma, T.; Ma, R.; Bao, Y.; Fan, Z. Numerical study of leakage characteristics of hydrogen-blended natural gas in buried pipelines. *Int. J. Hydrogen Energy* **2024**, *49*, 1166–1179. [\[CrossRef\]](#)
- Shirazi, M.; Fuinhas, J.A. Portfolio decisions of primary energy sources and economic complexity: The world's large energy user evidence. *Renew. Energy* **2023**, *202*, 347–361. [\[CrossRef\]](#)
- Nouri-Borujerdi, A.; Ziaei-Rad, M. Simulation of compressible flow in high pressure buried gas pipelines. *Int. J. Heat Mass Transf.* **2009**, *52*, 5751–5758. [\[CrossRef\]](#)
- Li, Y.; Wang, Z.; Shang, Z. Analysis and prediction of hydrogen-blended natural gas diffusion from various pipeline leakage sources based on CFD and ANN approach. *Int. J. Hydrogen Energy* **2024**, *53*, 535–549. [\[CrossRef\]](#)
- Berstad, T.; Dørum, C.; Jakobsen, J.P.; Kragset, S.; Li, H.; Lund, H.; Morin, A.; Munkejord, S.T.; Møltnvik, M.J.; Nordhagen, H.O.; et al. CO<sub>2</sub> pipeline integrity: A new evaluation methodology. *Energy Procedia* **2011**, *4*, 3000–3007. [\[CrossRef\]](#)
- Morin, A.; Kragset, S.; Munkejord, S.T. Pipeline flow modelling with source terms due to leakage: The straw method. In Proceedings of the 6th Trondheim Conference on CO<sub>2</sub> Capture, Transport and Storage (TCCS), Trondheim, Norway, 16–18 June 2012; pp. 226–235.
- Wu, T.; Jiang, N.; Zhou, C.; Luo, X.; Li, H.; Xia, Y. Dynamic response and safety assessment of buried gas pipe subjected to ground surface explosion. *Int. J. Press. Vessel. Pip.* **2021**, *194*, 104527. [\[CrossRef\]](#)
- Tong, S.; Li, X.; Ding, H.; Shuai, J.; Mei, Y.; Chan, S.H. Large-scale transient simulation for consequence analysis of hydrogen-doped natural gas leakage and explosion accidents. *Int. J. Hydrogen Energy* **2024**, *54*, 864–877. [\[CrossRef\]](#)



19. Oke, A.; Mahgerefteh, H.; Economou, I.; Rykov, Y. A transient outflow model for pipeline puncture. *Chem. Eng. Sci.* **2003**, *58*, 4591–4604. [[CrossRef](#)]
20. Ebrahimi-Moghadam, A.; Farzaneh-Gord, M.; Arabkoohsar, A.; Moghadam, A.J. CFD analysis of natural gas emission from damaged pipelines: Correlation development for leakage estimation. *J. Clean. Prod.* **2018**, *199*, 257–271. [[CrossRef](#)]
21. Mahgerefteh, H.; Oke, A.; Atti, O. Modelling outflow following rupture in pipeline networks. *Chem. Eng. Sci.* **2006**, *61*, 1811–1818. [[CrossRef](#)]
22. Scargiali, F.; Di Rienzo, E.; Ciofalo, M.; Grisafi, F.; Brucato, A. Heavy Gas Dispersion Modelling over a Topographically Complex Mesoscale: A CFD Based Approach. *Process Saf. Environ. Prot.* **2005**, *83*, 242–256. [[CrossRef](#)]
23. Zhu, H.; Mao, Z.; Wang, Q.; Sun, J. The Influences of Key Factors on the Consequences Following the Natural Gas Leakage from Pipeline. *Procedia Eng.* **2013**, *62*, 592–601. [[CrossRef](#)]
24. Liu, A.; Huang, J.; Li, Z.; Chen, J.; Huang, X.; Chen, K.; Xu, W.B. Numerical simulation and experiment on the law of urban natural gas leakage and diffusion for different building layouts. *J. Nat. Gas. Sci. Eng.* **2018**, *54*, 1–10. [[CrossRef](#)]
25. Holborn, P.G.; Benson, C.M.; Ingram, J.M. Modelling hazardous distances for large-scale liquid hydrogen pool releases. *Int. J. Hydrogen Energy* **2020**, *45*, 23851–23871. [[CrossRef](#)]
26. Wang, X.; Tan, Y.; Zhang, T.; Xiao, R.; Yu, K.; Zhang, J. Numerical study on the diffusion process of pinhole leakage of natural gas from underground pipelines to the soil. *J. Nat. Gas. Sci. Eng.* **2021**, *87*, 103792. [[CrossRef](#)]
27. Zhu, J.; Pan, J.; Zhang, Y.; Li, Y.; Li, H.; Feng, H.; Chen, D.; Kou, Y.; Yang, R. Leakage and diffusion behavior of a buried pipeline of hydrogen-blended natural gas. *Int. J. Hydrogen Energy* **2023**, *48*, 11592–11610. [[CrossRef](#)]
28. Lu, H.; Guo, B.; Chen, X.; Yao, J.; Liu, B. Numerical investigation on leakage and diffusion characteristics of buried hydrogen-blended natural gas pipelines. *Int. J. Hydrogen Energy* **2024**, *59*, 1491–1506. [[CrossRef](#)]
29. Cao, Z.; Hu, Y.; Chen, L.; Yan, X.; Yu, S.; Yu, J. Experimental study of leakage characteristics and risk prediction of N<sub>2</sub>-containing dense-phase CO<sub>2</sub> pipelines in real transportation conditions. *Process Saf. Environ. Prot.* **2024**, *187*, 1112–1125. [[CrossRef](#)]
30. Zhang, B.; Chen, G.-m. Quantitative risk analysis of toxic gas release caused poisoning—A CFD and dose–response model combined approach. *Process Saf. Environ. Prot.* **2010**, *88*, 253–262. [[CrossRef](#)]
31. Bagheri, M.; Alamdari, A.; Davoudi, M. Quantitative risk assessment of sour gas transmission pipelines using CFD. *J. Nat. Gas. Sci. Eng.* **2016**, *31*, 108–118. [[CrossRef](#)]
32. Peng, S.; Zhang, Z.; Liu, E.; Liu, W.; Qiao, W. A new hybrid algorithm model for prediction of internal corrosion rate of multiphase pipeline. *J. Nat. Gas. Sci. Eng.* **2021**, *85*, 103716. [[CrossRef](#)]
33. Liu, E.B.; Wang, X.J.; Zhao, W.W.; Su, Z.Y.; Chen, Q.K. Analysis and Research on Pipeline Vibration of a Natural Gas Compressor Station and Vibration Reduction Measures. *Energy Fuels* **2021**, *35*, 479–492. [[CrossRef](#)]
34. Liu, E.; Lu, X.; Wang, D. A Systematic Review of Carbon Capture, Utilization and Storage: Status, Progress and Challenges. *Energies* **2023**, *16*, 2865. [[CrossRef](#)]
35. Liu, E.-B.; Peng, Y.; Peng, S.-B.; Yu, B.; Chen, Q.-K. Research on low carbon emission optimization operation technology of natural gas pipeline under multi-energy structure. *Pet. Sci.* **2022**, *19*, 3046–3058. [[CrossRef](#)]
36. Kou, B.; Liu, E.B.; Li, D.J.; Qiao, W.B.; Chen, R.L.; Peng, S.B. Research on Erosion Characteristics of the Sleeve-Type Blowdown Valve in the Shale Gas Gathering and Transportation Station. *SPE J.* **2024**, *29*, 328–345. [[CrossRef](#)]

**Disclaimer/Publisher’s Note:** The statements, opinions and data contained in all publications are solely those of the individual author(s) and contributor(s) and not of MDPI and/or the editor(s). MDPI and/or the editor(s) disclaim responsibility for any injury to people or property resulting from any ideas, methods, instructions or products referred to in the content.